Research Article | Vol. 29, No. 15 / 19 July 2021 / Optics Express 23508
Optics EXPRESS

Fast thermo-optical modulators with doped-silicon heaters operating at 2 μm

CHUYU ZHONG,[1] HUI MA,[1] CHUNLEI SUN,[2,3] MAOLIANG WEI,[1] YUTING YE,[2,3] BO TANG,[4] PENG ZHANG,[4] RUONAN LIU,[4] JUNYING LI,[1] LAN LI,[2,3] AND HONGTAO LIN[1,*]

[1]State Key Laboratory of Modern Optical Instrumentation, College of Information Science and Electronic Engineering, Zhejiang University, Hangzhou 310027, China
[2]Key Laboratory of 3D Micro/Nano Fabrication and Characterization of Zhejiang Province, School of Engineering, Westlake University, Hangzhou, Zhejiang 310024, China
[3]Institute of Advanced Technology, Westlake Institute for Advanced Study, Hangzhou, Zhejiang 310024, China
[4]Institute of Microelectronics of the Chinese Academy of Sciences, Beijing 100029, China
*hometown@zju.edu.cn

Abstract: The 2-μm-waveband has been recognized as a potential telecommunication window for next-generation low-loss, low-latency optical communication. Thermo-optic (TO) modulators and switches, which are essential building blocks in a large-scale integrated photonic circuit, and their performances directly affect the energy consumption and reconfiguration time of an on-chip photonic system. Previous TO modulation based on metallic heaters at 2-μm-waveband suffer from slow response time and high power consumption. In this paper, high-performance thermo-optical Mach–Zehnder interferometer and ring resonator modulators operating at 2-μm-waveband were demonstrated. By embedding a doped silicon (p_{++}-p-p_{++}) junction into the waveguide, our devices reached a record modulation efficiency of 0.17 nm/mW for Mach–Zehnder interferometer based modulator and its rise/fall time was 3.49 μs/3.46 μs which has been the fastest response time reported in a 2-μm-waveband TO devices so far. And a lowest P_π power of 3.33 mW among reported 2-μm TO devices was achieved for a ring resonator-based modulator.

1. Introduction

With the development of artificial intelligence, the Internet of Things, and other information technology, current fiber telecommunication systems are foreseeably reaching their capacity limit. Extending the optical communication window to a new wavelength range has been proposed to be a potential solution. The emergence of Thulium-/Holmium-doped fiber amplifiers (TDFAs/HDFAs) [1] with ultra-wideband (1.85-2.05 μm), low-noise, and high gain makes the 2-μm-waveband favorable as the new telecommunication window for wavelength-division-multiplexing systems. Besides, hollow-core photonic bandgap fibers (HC-PBGF) [2,3] could potentially achieve a loss as low as 0.2 dB/km at 2-μm wavelength band and allow high-capacity and low-latency data transmission because of their intriguing optical properties, including high damage threshold and significantly reduced nonlinearity and dispersion. All these facts make it worthwhile to explore the 2-μm-waveband as a potential window for future telecommunications and data communications. Silicon photonic devices have recently attracted an increasing amount of attention to building up the 2-μm communication infrastructure. A series of devices such as arrayed waveguide gratings [4,5], lasers [6,7], modulators [8,9], photodetectors [10,11], mode multiplexers [12], power splitters [13], and other key components at this waveband had been developed. In spite of that, essential components, such as high-performance optic switches, remain to be further investigated for a complete integrated photonic circuit at 2-μm-waveband.

#430756 https://doi.org/10.1364/OE.430756
Journal © 2021 Received 11 May 2021; revised 23 Jun 2021; accepted 30 Jun 2021; published 9 Jul 2021

Optics EXPRESS

Optical modulators and switches can flexibly define the data throughput and the light path in optical links [14], and their reconfiguration time and power consumption limit the overall performance of optical communication systems operating in the 2-μm-wavelength range. Electro-optic (EO) modulators exhibit high speed but suffer from low modulation efficiency and large footprints, whereas thermo-optic (TO) modulators and switches provide a moderate speed, compact and low-loss solution that facilitates large-scale photonic integration. The high thermo-optic coefficient of silicon makes it an excellent platform for integrated TO modulation. A variety of applications, including light detection and ranging (LIDAR) [15], on-chip spectroscopy [16], photonic computing [17], and quantum computing [18], were achieved based on TO switches at 1.55 μm. Thus, high-performance complementary metal-oxide-semiconductor (CMOS)-compatible silicon TO modulators and switches at 2-μm-waveband deserve further exploration because of the very limited number of studies reported so far.

The key unit for a TO modulator is the microheater, which can be a metallic heater [19], a silicide heater [20], or a doped silicon heater [21,22]. For ease of comparison, a figure-of-merit (FOM) of TO modulator could be defined as $1/(P_\pi \cdot \tau)$, in which P_π is the π-phase-shift power consumption and τ is the response time [23] (choose the longer τ if the rise time and fall time are not identical as the longer response time limits the dynamic performance). TiN heaters have been utilized in TO switches at 2-μm-waveband [24–26]. However, the metallic heaters are usually placed at least 1 μm above the waveguide by silica spacers to suppress the parasitic optical absorption. The thick silica spacer inevitably impedes the heat conduction from the heater to the waveguide below due to its low thermal conductivity. Thus, these external heaters often experience severe heat dissipation to surrounding cladding and a large heat capacitance, which leads to relatively high power consumption, low response time, and a typical FOM of around 0.001 $mW^{-1}\mu s^{-1}$. On the contrary, the current could flow through the doped Si heater [21,22], which generates Joule heat directly inside optical waveguides without long-distance heat transportation. This enables TO switches based on doped silicon heaters to achieve a relatively high FOM with a fast response time and reduced power consumption. However, TO modulators or switches based on doped silicon operated at the 2-μm-waveband have not been demonstrated yet.

In this paper, we demonstrated high-performance thermo-optic modulators with p_{++}-p-p_{++}-type silicon heaters at 2-μm-waveband based on a 220 nm silicon-on-insulator (SOI) platform for the first time. Mach-Zehnder interferometers (MZIs) and micro-ring resonators (MRR) were used to improve the optical modulation performance. Our MZI-based TO modulator showed a high modulation depth of 17 dB, low insertion loss of 1.13 dB, and a fast response time of 3.49/3.46 μs. As for our proposed MRR-based TO modulator, it achieved low P_π power consumption of 3.3 mW and exhibited a high FOM of 0.081 $mW^{-1}\mu s^{-1}$. These proposed TO modulators can further promote large-scale photonic integration at 2 μm significantly.

2. Structure design and thermo-electric and optical simulation of the p_{++}-p-p_{++} heater

The schematic cross-section and key structural parameters of the p_{++}-p-p_{++} structure are shown in Fig. 1(a). Our devices were fabricated on a 220 nm SOI wafer, where the waveguide width is 0.6 μm, and the ridge height is 0.15 μm. The lightly doped areas are 1.5-μm-wide, and the heavily doped areas are 0.45 μm away from the edges of the waveguide to suppress the free carrier absorption loss. The contacts are 3.7 μm away from the waveguide edges, preventing the excessive absorption from metal contacts.

The 2D temperature distribution in the p_{++}-p-p_{++} structure was simulated by the COMSOL Multiphysics thermo-electric solver. The boundary conditions with constant room temperature at the boundaries of the silicon substrate and convective heat flux at the boundaries of the open-air

Optics EXPRESS

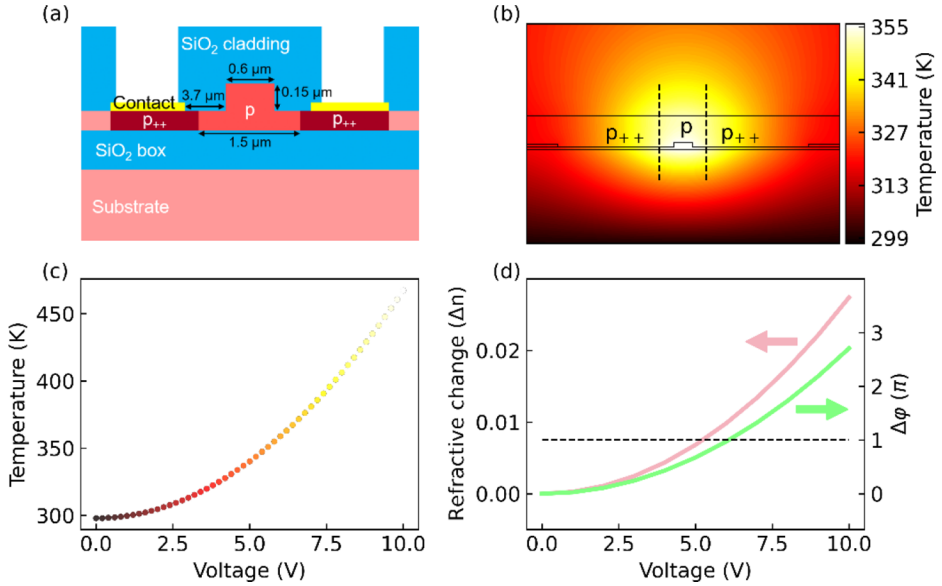

Fig. 1. (a) Schematic cross-section of the p_{++}-p-p_{++} structure. (b) Simulated temperature distribution in the p-type-doped heater at a driving voltage of 5.8 V. (c) Simulated temperature in the waveguide under different voltages. (d) Voltage-dependent effective refractive index change and phase shift. The dashed line denotes the π-shift position.

region were set. The simulated temperature distribution depicted in Fig. 1(b) was obtained at a driving voltage of 5.8 V. The temperature of the waveguide core could be heated up to 355.46 K.

The phase tuning $\Delta\varphi$ as a function of temperature variation can be expressed as $\Delta\varphi = \frac{2\pi L}{\lambda_0}\frac{dn}{dT}\Delta T$ [23,27] where λ_0 is the free-space wavelength, L is the heating length, dn/dT is the TO coefficient, approximately 1.76×10^{-4} K^{-1} [28] for silicon at 2 μm under room-temperature, and ΔT is the variation of temperature. Figures 1(c) and 1(d) demonstrate the calculated temperature in the waveguide, effective refractive index change and phase shift under different voltages, respectively. Therefore, for a 100-μm-long waveguide phase shifter, a temperature change of 57.53 K is needed to produce one π-shift at 2 μm.

3. Fabrication processes and measurement setup

The devices were fabricated on 220 nm SOI wafers with a 2-μm-thick SiO_2 box layer in a multistep process with multi-project-wafer (MPW) runs involved at the Institute of Microelectronics of the Chinese Academy of Sciences (IMECAS). Firstly, the waveguide patterns were defined by deep ultra-violet (DUV) photolithography and inductive coupling plasma (ICP) etching process. Secondly, boron ion implantation was performed to form the lightly doped *p*-type areas with a doping concentration of 7×10^{17} cm^{-3} followed by a heavy doping process with a doping concentration of 1.7×10^{20} cm^{-3}. Thirdly, the Ti/Au (5 nm/100 nm) contact electrodes patterned by electron beam lithography (EBL) were deposited directly above the heavily doped areas using electron beam evaporation to form the ohmic contact. Finally, a 1-μm-thick SiO_2 cladding was deposited by plasma-enhanced chemical vapor deposition (PECVD), and electrode windows were opened by hydrofluoric acid etching.

The measurement system is shown in Fig. 2. The computer controlled the tunable 2 μm laser's wavelength sweeping and processed the data stream from the data acquisition equipment (DAQ), which was used for data synchronization between the laser and the power meter. The polarization of the light was adjusted by a polarization controller (PC) to optimize the coupling efficiency. And

Optics EXPRESS

the transmitted optical signal was read by the power meter. For static measurement, a source meter was used to apply voltage and monitor the current flowed through the p-doped heaters. The peak shift of the devices and I-V/O-P(current-voltage/transmission-power) curves could be obtained. For dynamic characterization, an arbitrary waveform generator (AWG, Siglent SDG6032X-E) was utilized to apply the modulation signal. The optical output of the device was connected to a photodetector, while its photocurrent was amplified by a photomultiplier-tube (PMT-PFA). The amplified modulated signal was recorded by an oscilloscope (Siglent SDS5104X) in real time. In this way, the rise and fall times of our devices could be obtained.

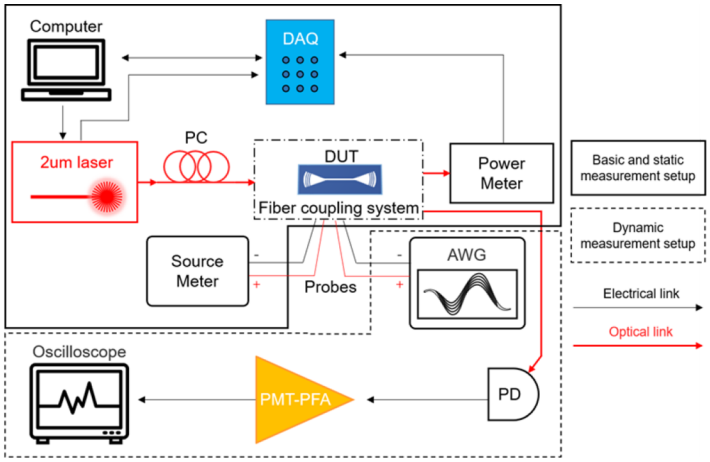

Fig. 2. Schematic of the measurement system: a fiber coupling setup is used for light coupling. DAQ: data acquisition equipment, PC: polarization controller, DUT: device under test, AWG: arbitrary waveform generator, PD: photodetector, PMT: photomultiplier tube, PFA: pulse forming amplifier.

4. High-performance silicon TO modulators at 2 μm

4.1. MZI-based modulators

We designed and fabricated unbalanced MZI TO modulators with the heaters on one of the MZI arms. The microscope view of the modulator is shown in Fig. 3(a). The inset shows a zoom-in view of the p-doped heating structure. The modulator achieved a low insertion loss of about 1.13 dB [Fig. 3(b)], which is obtained by subtracting the transmission of the MZI device from the reference waveguide device. The insertion loss comes from the MMIs and the doped waveguide (~19.5 dB/cm, measured from ring resonators), and it could be further reduced by improving the fabrication process in the future. When applying the driving voltage on a 100-μm-long p-doped heater, the current in the junction and the transmittance at 2005 nm were measured simultaneously, as shown in Fig. 3(c). As the applied voltage increases, the peaks of the TO modulator show a red shift [Fig. 3(b)] due to the phase shift induced by the refractive index change in one of the MZI arms. The modulator realized an on-off ratio of 17 dB. As Fig. 3(d) shows, the energy efficiency η of the modulator was calculated to be 0.17 nm/mW, and the free spectral range (FSR) of the MZI was about 8.5 nm. Therefore, the π-shift power consumption P_π ($P_\pi = \mathrm{FSR}/2/\eta$) was calculated to be 25.21 mW as depicted in Fig. 3(d).

The dynamic response of the modulator was also characterized. As shown in Fig. 4, by applying a square-wave driven signal with an amplitude of 5.2 V, a frequency of 40 kHz and a duty cycle of 50%, the MZI TO modulator achieved a 10%-90% rise time of 3.49 μs and a 90%-10% fall time of 3.46 μs at the wavelength of 2023 nm, which is the fastest 2-μm TO

Optics EXPRESS

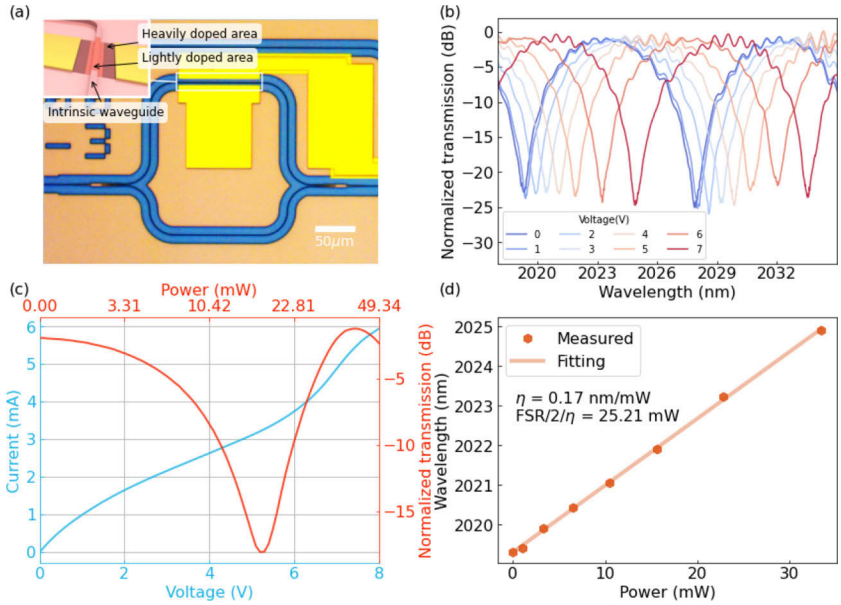

Fig. 3. (a) The structure of the MZI-based TO modulator. (b) Normalized transmission spectra of the modulator under varying applied voltages. (c) Measured Current-Voltage (I-V, light-blue) and Transmission-Power (O-P, red) curves of the p_{++}-p-p_{++} junction in the modulator. (d) The wavelength shift of the interference dip of the modulator with the heating power.

modulator ever reported (Table 1). Thus, the FOM of the modulator is calculated to be 0.011 $mW^{-1}\mu s^{-1}$.

4.2. MRR-based modulators

To further minimize the device footprint and power consumption, we embedded the p-doped heater into the micro-ring resonator with a radius of 40 μm. A microscope image of the MRR-based TO modulator is shown in Fig. 5(a). The resonance wavelengths of measured transmission spectra red shifted as shown in Fig. 5(b). The length of p-doped waveguide is 50 μm, and the measured IV curve is shown in Fig. 5(c), manifesting similar characteristics of the junctions. The energy efficiency of the modulator was calculated to be 0.1 nm/mW [Fig. 5(d)]. Benefiting from the enhanced light trapping inside the ring resonator, the O-P curve of the modulator in Fig. 5(c) possesses a sharper dip than that of the MZI-based modulator. The modulator claims a P_π of 3.33 mW, where P_π of a cavity-type modulator is defined as the power consumption to detune the resonator by a phase shift with a product of π and full width at half maximum (FWHM, 0.11 nm for our device at 0 V) of the resonance peak (P_π = FWHM*π/η) [23]. To the best of our knowledge, the power consumption is among the lowest values in on-chip 2 μm TO modulators up to date, which mainly benefits from the enhancement of the optical field in the active area in the MRR with a quality factor of 1.8×10^4.

As demonstrated in Fig. 6, the modulation waveform is fitted. The 10%-90% rise and 90%-10% fall time of the modulator are 3.65 μs and 3.70 μs, respectively, via applying a 1.7 V square-wave driven signal with a frequency of 40 kHz and a duty cycle of 0.5. The modulator realized a FOM record as high as 0.081 $mW^{-1}\mu s^{-1}$.

Optics EXPRESS

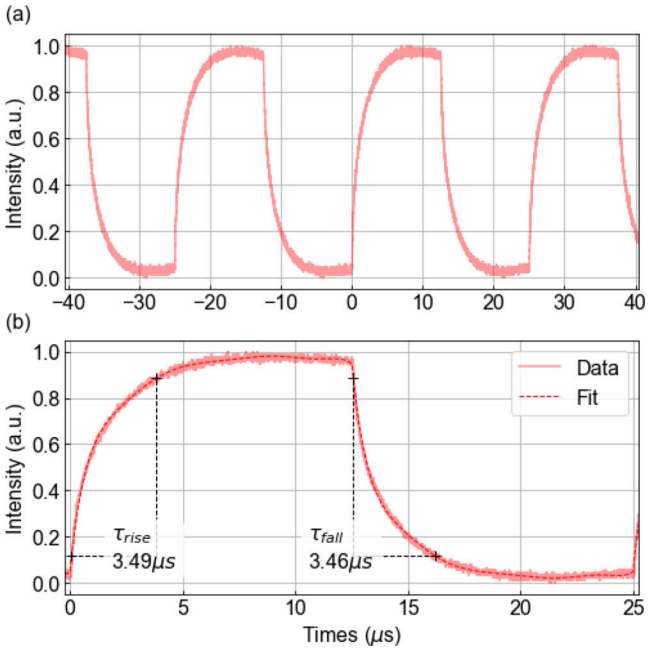

Fig. 4. Time response of the MZI-based 2-μm-waveband TO modulator.

4.3. Discussion

We summarize the performance of silicon TO modulators with p-doped heaters in this work and previously reported 1.55-μm- and 2-μm-waveband TO modulators or switches, as shown in Table 1. The MZI-based TO modulator in this work demonstrated a FOM much higher than that of MZI-based TO switches with TiN metallic heaters [24,25,29]. Our MZI-based TO switch indicates a faster rise time since the designed p_{++}-p-p_{++}-type heater directly heats

Table 1. Performance of Some Reported Silicon TO Modulation Devices

Device	Wavelength (nm)	Energy Efficiency (nm/mW)	Rise/Fall time τ (μs)	Power P_π (mW)	FOM ($mW^{-1}\mu s^{-1}$)	Year (Ref.)
MZI switch with doped silicon heater	1550	N/A	5.3/-	12.7	0.015	2013 [30]
MZI modulator with doped silicon heater	1550	0.25	2.69/-	24.8	0.015	2014 [27]
MZI switch with doped-silicon heater	1550	N/A	2.16/2.08	28	0.016	2019 [31]
Add-drop MRR switch with TiN heater	1980	0.17	N/A	N/A	N/A	2018 [24]
MZI switch with TiN heater	2000	N/A	15/15	32.3	0.002	2019 [25]
Dual-mode switch with TiN heater	2000	N/A	9.2/13.2	19.2	0.004	2021 [29]
MZI with p-doped silicon heater	2023	0.17	3.49/3.46	25.21	0.011	2021 this work
MRR with p-doped silicon heater	2024	0.1	3.65/3.70	3.33	0.081	2021 this work

Optics EXPRESS

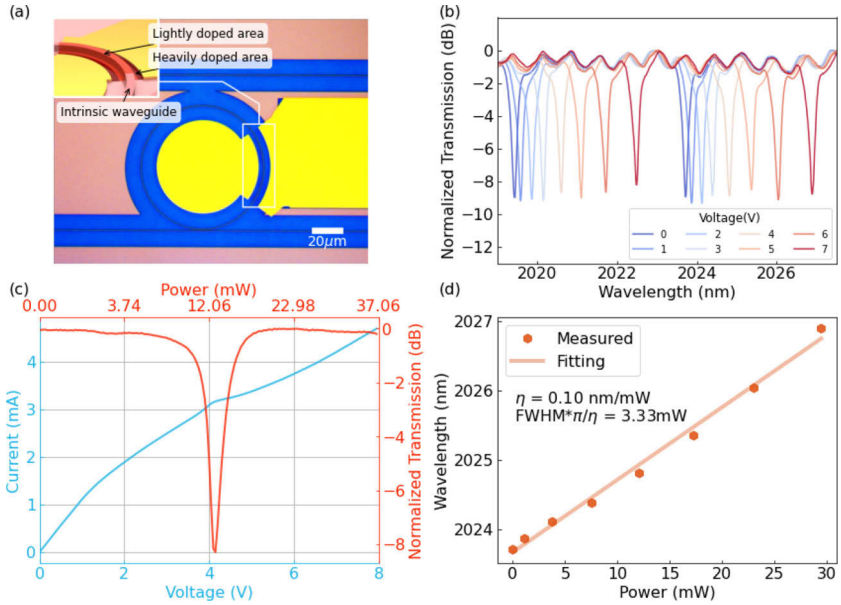

Fig. 5. (a) The structure of the MRR-based TO with p-doped heaters. (b) Normalized transmission spectra of the modulator under varying applied voltage. (c) I-V and O-P curves of the p_{++}-p-p_{++} junction in the modulator. (d) Resonant peak shift of the modulator with the heating power.

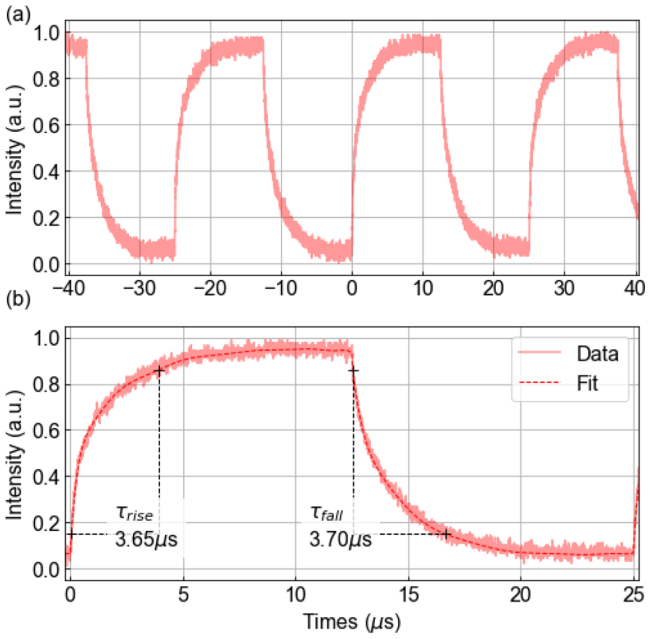

Fig. 6. Time response of the MRR-based TO modulator.

the Si waveguide instead of utilizing the heat conducted from silica spacer with low thermal conductivity. Meanwhile, the *p*-doped-heater-embedded MRR-based TO modulator in this work realized not only a fast TO rise time of 3.65 μs, but also very low power consumption of 3.33

Optics EXPRESS

mW. The TO FOM was nearly an order of magnitude higher than our MZI-based TO modulator and one order of magnitude higher than previously reported TiN-heater-assisted TO switches.

5. Conclusion

We demonstrated MZI-based and MRR-based TO switches operating at 2-μm-waveband, where *p*-doped silicon structures were adopted as the phase shifters. For the MZI-based TO modulator, the modulation efficiency was 0.17 nm/mW, corresponding to the π-shift power consumption of about 25.21 mW. As for the MRR-based one, the modulation efficiency was 0.1 nm/mW while low P_π power consumption of 3.33 mW was achieved because of the resonant enhancement effect. The dynamic response of our devices was also measured. The 10%-90% rise time/90%-10% fall time is 3.49 μs/3.46 μs in MZI-based TO switch and 3.65 μs/3.70 μs in MRR-based one, respectively, exhibiting the highest performance of TO devices operating at 2 μm so far. Thus, TO modulators with p-doped silicon heaters, possessing the potential to minimize power consumption without restricting the response speed, may play an important role in promoting next-generation low-loss, low-latency optical communication at 2-μm-waveband.

Funding. National Key Research and Development Program of China (2019YFB2203003); National Natural Science Foundation of China (61975179, 91950204); Open Fund of State Key Laboratory on Integrated Optoelectronics (IOSKL2020KF05); Fundamental Research Funds for the Central Universities (2020XZZX005-07, 2021QNA5007).

Acknowledgments. The authors would like to acknowledge the fabrication support from Institute of Microelectronics of the Chinese Academy Sciences, ZJU Micro-Nano Fabrication Center in Zhejiang University and Westlake Center for Micro/Nano Fabrication in Westlake University.

Disclosures. The authors declare no conflicts of interest.

Data availability. Data underlying the results presented in this paper are not publicly available at this time but may be obtained from the authors upon reasonable request.

References

1. Z. Li, A. M. Heidt, J. M. Daniel, Y. Jung, S. U. Alam, and D. J. Richardson, "Thulium-doped fiber amplifier for optical communications at 2 microm," Opt. Express **21**(8), 9289–9297 (2013).
2. M. U. Sadiq, H. Zhang, J. O'Callaghan, B. Roycroft, N. Kavanagh, K. Thomas, A. Gocalinska, Y. Chen, T. Bradley, J. R. Hayes, Z. Li, S.-U. Alam, F. Poletti, M. N. Petrovich, D. J. Richardson, E. Pelucchi, P. O'Brien, F. H. Peters, F. Gunning, and B. Corbett, "40 Gb/s WDM transmission over 1.15-km HC-PBGF using an InP-based Mach-Zehnder modulator at 2 μm," J. Lightwave Technol. **34**(8), 1706–1711 (2016).
3. W. Shen, J. Du, L. Sun, C. Wang, Y. Zhu, K. Xu, B. Chen, and Z. He, "Low-latency and high-speed hollow-core biber optical interconnection at 2-micron waveband," J. Lightwave Technol. **38**(15), 3874–3882 (2020).
4. Y. Liu, Z. Li, D. Li, Y. Yao, J. Du, Z. He, and K. Xu, "Thermo-optic tunable silicon arrayed waveguide grating at 2-μm wavelength band," IEEE Photonics J. **12**(4), 1–8 (2020).
5. E. J. Stanton, N. Volet, and J. E. Bowers, "Silicon arrayed waveguide gratings at 2.0-μm wavelength characterized with an on-chip resonator," Opt. Lett. **43**(5), 1135–1138 (2018).
6. R. Wang, S. Sprengel, G. Boehm, R. Baets, M.-C. Amann, and G. Roelkens, "Broad wavelength coverage 2.3 μm III-V-on-silicon DFB laser array," Optica **4**(8), 972–975 (2017).
7. R. Wang, S. Sprengel, A. Vasiliev, G. Boehm, J. Van Campenhout, G. Lepage, P. Verheyen, R. Baets, M.-C. Amann, and G. Roelkens, "Widely tunable 2.3 μm III-V-on-silicon Vernier lasers for broadband spectroscopic sensing," Photonics Res. **6**(9), 858–866 (2018).
8. W. Cao, D. Hagan, D. J. Thomson, M. Nedeljkovic, C. G. Littlejohns, A. Knights, S.-U. Alam, J. Wang, F. Gardes, W. Zhang, S. Liu, K. Li, M. S. Rouifed, G. Xin, W. Wang, H. Wang, G. T. Reed, and G. Z. Mashanovich, "High-speed silicon modulators for the 2 μm wavelength band," Optica **5**(9), 1055–1062 (2018).
9. X. Wang, W. Shen, W. Li, Y. Liu, Y. Yao, J. Du, Q. Song, and K. Xu, "High-speed silicon photonic Mach–Zehnder modulator at 2 μm," Photonics Res. **9**(4), 535–540 (2021).
10. J. J. Ackert, D. J. Thomson, L. Shen, A. C. Peacock, P. E. Jessop, G. T. Reed, G. Z. Mashanovich, and A. P. Knights, "High-speed detection at two micrometres with monolithic silicon photodiodes," Nat. Photonics **9**(6), 393–396 (2015).
11. M. Casalino, R. Russo, C. Russo, A. Ciajolo, E. Di Gennaro, M. Iodice, and G. Coppola, "Free-Space Schottky Graphene/Silicon Photodetectors Operating at 2 μm," ACS Photonics **5**(11), 4577–4585 (2018).
12. S. Zheng, M. Huang, X. Cao, L. Wang, Z. Ruan, L. Shen, and J. Wang, "Silicon-based four-mode division multiplexing for chip-scale optical data transmission in the 2 μm-waveband," Photonics Res. **7**(9), 1030–1035 (2019).
13. H. Xie, Y. Liu, W. Sun, Y. Wang, K. Xu, J. Du, Z. He, and Q. Song, "Inversely designed 1 × 4 power splitter with arbitrary ratios at 2-μm spectral band," IEEE Photonics J. **10**(4), 1–6 (2018).

Optics EXPRESS

14. Q. X. Cheng, M. Bahadori, M. Glick, S. Rumley, and K. Bergman, "Recent advances in optical technologies for data centers: a review," Optica **5**(11), 1354–1370 (2018).
15. T. Kim, P. Bhargava, C. V. Poulton, J. Notaros, A. Yaacobi, E. Timurdogan, C. Baiocco, N. Fahrenkopf, S. Kruger, T. Ngai, Y. Timalsina, M. R. Watts, and V. Stojanovic, "A single-chip optical phased array in a 3D-integrated silicon photonics/65 nm CMOS technology," *IEEE International Solid-State Circuits Conference (ISSCC)* (2019), pp. 464–466.
16. D. M. Kita, B. Miranda, D. Favela, D. Bono, J. Michon, H. Lin, T. Gu, and J. Hu, "High-performance and scalable on-chip digital Fourier transform spectroscopy," Nat. Commun. **9**(1), 4405 (2018).
17. Y. Shen, N. C. Harris, S. Skirlo, M. Prabhu, T. Baehr-Jones, M. Hochberg, X. Sun, S. Zhao, H. Larochelle, D. Englund, and M. Soljačić, "Deep learning with coherent nanophotonic circuits," Nat. Photonics **11**(7), 441–446 (2017).
18. N. C. Harris, G. R. Steinbrecher, M. Prabhu, Y. Lahini, J. Mower, D. Bunandar, C. Chen, F. N. C. Wong, T. Baehr-Jones, M. Hochberg, S. Lloyd, and D. Englund, "Quantum transport simulations in a programmable nanophotonic processor," Nat. Photonics **11**(7), 447–452 (2017).
19. L. Zeqin, K. Murray, H. Jayatilleka, and L. Chrostowski, "Michelson interferometer thermo-optic switch on SOI with a 50-μw power consumption," IEEE Photonics Technol. Lett. **27**(22), 2319–2322 (2015).
20. J. Van Campenhout, W. M. Green, S. Assefa, and Y. A. Vlasov, "Integrated NiSi waveguide heaters for CMOS-compatible silicon thermo-optic devices," Opt. Lett. **35**(7), 1013–1015 (2010).
21. P. Dong, W. Qian, H. Liang, R. Shafiiha, D. Feng, G. Li, J. E. Cunningham, A. V. Krishnamoorthy, and M. Asghari, "Thermally tunable silicon racetrack resonators with ultralow tuning power," Opt. Express **18**(19), 20298–20304 (2010).
22. D. Englund, B. Ellis, E. Edwards, T. Sarmiento, J. S. Harris, D. A. Miller, and J. Vuckovic, "Electrically controlled modulation in a photonic crystal nanocavity," Opt. Express **17**(18), 15409–15419 (2009).
23. H. Lin, Y. Song, Y. Huang, D. Kita, S. Deckoff-Jones, K. Wang, L. Li, J. Li, H. Zheng, Z. Luo, H. Wang, S. Novak, A. Yadav, C.-C. Huang, R.-J. Shiue, D. Englund, T. Gu, D. Hewak, K. Richardson, J. Kong, and J. Hu, "Chalcogenide glass-on-graphene photonics," Nat. Photonics **11**(12), 798–805 (2017).
24. J. Li, Y. Liu, Y. Meng, K. Xu, J. Du, F. Wang, Z. He, and Q. Song, "2-μm Wavelength Grating Coupler, Bent Waveguide, and Tunable Microring on Silicon Photonic MPW," IEEE Photonics Technol. Lett. **30**(5), 471–474 (2018).
25. L. Shen, M. Huang, S. Zheng, L. Yang, X. Peng, X. Cao, S. Li, and J. Wang, "High-Performance Silicon 2 × 2 Thermo-Optic Switch for the 2-um Wavelength Band," IEEE Photonics J. **11**(4), 1–6 (2019).
26. J. X. B. Sia, X. Li, Z. Qiao, X. Guo, J. Zhou, C. G. Littlejohns, C. Liu, G. T. Reed, W. Wang, and H. Wang, "1 × N (N = 2, 8) silicon selector wwitch for prospective technologies at the 2 μm-waveband," IEEE Photonics Technol. Lett. **32**(18), 1 (2020).
27. N. C. Harris, Y. Ma, J. Mower, T. Baehr-Jones, D. Englund, M. Hochberg, and C. Galland, "Efficient, compact and low loss thermo-optic phase shifter in silicon," Opt. Express **22**(9), 10487–10493 (2014).
28. E. Atad-Ettedgui, B. J. Frey, J. Antebi, D. B. Leviton, T. J. Madison, and D. Lemke, "Temperature-dependent refractive index of silicon and germanium," in *Optomechanical Technologies for Astronomy* 6273 (SPIE 2006), p. 62732H.
29. W. Shen, J. Du, K. Xu, and Z. He, "On-Chip Selective Dual-Mode Switch for 2-μm Wavelength High-Speed Optical Interconnection," IEEE Photonics Technol. Lett. **33**(10), 483–486 (2021).
30. M. R. Watts, J. Sun, C. DeRose, D. C. Trotter, R. W. Young, and G. N. Nielson, "Adiabatic thermo-optic Mach-Zehnder switch," Opt. Lett. **38**(5), 733–735 (2013).
31. M. Mendez-Astudillo, M. Okamoto, Y. Ito, and T. Kita, "Compact thermo-optic MZI switch in silicon-on-insulator using direct carrier injection," Opt. Express **27**(2), 899–906 (2019).